Bioorganic & Medicinal Chemistry 17 (2009) 6761–6772

Contents lists available at ScienceDirect

Bioorganic & Medicinal Chemistry

journal homepage: www.elsevier.com/locate/bmc

Synthesis and molecular modeling of some novel hexahydroindazole derivatives as potent monoamine oxidase inhibitors

Nesrin Gökhan-Kelekçi [a,*], Ö. Özgün Şimşek [a], Ayşe Ercan [b], Kemal Yelekçi [c], Z. Sibel Şahin [d], Şamil Işık [d], Gülberk Uçar [b], A. Altan Bilgin [a]

[a] Faculty of Pharmacy, Department of Pharmaceutical Chemistry, Hacettepe University, 06100 Sıhhıye, Ankara, Turkey
[b] Faculty of Pharmacy, Department of Biochemistry, Hacettepe University, 06100 Sıhhıye, Ankara, Turkey
[c] Kadir Has University, The Faculty of Arts and Sciences, 34080 Fatih-İstanbul, Turkey
[d] Ondokuz MayısUniversity, Faculty of Arts and Sciences,, Department of Physics, 55139 Kurupelit, Samsun, Turkey

ARTICLE INFO

Article history:
Received 2 February 2009
Revised 8 July 2009
Accepted 16 July 2009
Available online 23 July 2009

Keywords:
Hexahydroindazole
MAO-A/MAO-B inhibition
Docking
X-ray crystallographic model

ABSTRACT

A novel series of 2-thiocarbamoyl-2,3,4,5,6,7-hexahydro-1*H*-indazole and 2-substituted thiocarbamoyl-3,3a,4,5,6,7-hexahydro-2*H*-indazoles derivatives were synthesized and investigated for the ability to inhibit the activity of the A and B isoforms of monoamine oxidase (MAO). The target molecules were identified on the basis of satisfactory analytical and spectra data (IR, ^{1}H NMR, ^{13}C NMR, ^{2}D NMR, DEPT, EI-MASS techniques and elemental analysis). Synthesized compounds showed high activity against both the MAO-A (compounds **1d**, **1e**, **2c**, **2d**, **2e**) and the MAO-B (compounds **1a**, **1b**, **1c**, **2a**, **2b**) isoforms. In the discussion of the results, the influence of the structure on the biological activity of the prepared compounds was delineated. It was suggested that non-substituted and *N*-methyl/ethyl bearing compounds (except **2c**) increased the inhibitory effect and selectivity toward MAO-B. The rest of the compounds, carrying *N*-allyl and *N*-phenyl, appeared to select the MAO-A isoform. The inhibition profile was found to be competitive and reversible for all compounds. A series of experimentally tested (**1a**–**2e**) compounds was docked computationally to the active site of the MAO-A and MAO-B isoenzyme. The AUTODOCK 4.01 program was employed to perform automated molecular docking. In order to see the detailed interactions of the docked poses of the model inhibitors compounds **1a**, **1d**, **1e** and **2e** were chosen because of their ability to reversibly inhibit the MAO-B and MAO-A and the availability of experimental inhibition data. The differences in the intermolecular hydrophobic and H-bonding of ligands to the active site of each MAO isoform were correlated to their biological data. Observation of the docked positions of these ligands revealed interactions with many residues previously reported to have an effect on the inhibition of the enzyme. Excellent to good correlations between the calculated and experimental K_i values were obtained. In the docking of the MAO-A complex, the *trans* configuration of compound **1e** made various very close interactions with the residues lining the active site cavity these interactions were much better than those of the other compounds tested in this study. This tight binding observation may be responsible for the nanomolar inhibition of form of MAOA. However, it binds slightly weaker (experimental K_i = 1.23 μM) to MAO-B than to MAO-A (experimental K_i = 4.22 nM).

1. Introduction

Amine oxidases (amine: oxygen oxidoreductases, AOs) are a heterogeneous superfamily of enzymes that catalyze the oxidative deamination of mono-, di-, and polyamines. AOs differ because of their molecular architecture, catalytic mechanisms and subcellular localizations. On the basis of the chemical nature of the cofactor, AOs fall into two classes: AOs that contain flavin adenine dinucleotide as a cofactor (FAD-AOs), and semicarbazide sensitive AOs (ssAOs) that contain copper II-2,4,5-trihydroxyphenylalanine quinone as a cofactor (TPQ-Cu AOs). Both classes have been isolated and characterized from micro-organisms, plants and mammals. Monoamine oxidase (MAO, E.C. 1.4.3.4) is a flavin adenine dinucleotide (FAD)-containing enzyme present in the outer mitochondrial membranes of neuronal, glial and other cells.[1–3] It catalyzes the oxidative deamination of biogenic amines in the brain and the peripheral tissues, regulating their level. MAO exists in two forms, namely, MAO-A and MAO-B.[4] MAO-A catalyzes the oxidative deamination of serotonin (5-HT), adrenaline (A), and noradrenaline (NA) and is selectively inhibited by irreversible inhibitor clorgyline and reversible inhibitor moclobemide. MAO-B catalyzes the

* Corresponding author. Tel.: +90 312 305 30 17; fax: +90 312 311 47 77.
E-mail address: onesrin@hacettepe.edu.tr (N. Gökhan-Kelekçi).

0968-0896/$ - see front matter © 2009 Elsevier Ltd. All rights reserved.
doi:10.1016/j.bmc.2009.07.033

oxidative deamination of β-phenylethylamine and benzylamine and is selectively inhibited by irreversible inhibitor selegiline.[5]

MAO-A and MAO-B have essential roles in vital physiological processes and are involved in the pathogenesis of various human diseases. Due to their key role, MAO inhibitors represent a useful tool for the treatment of several psychiatric and neurological diseases. In particular, reversible and selective MAO-A inhibitors are used as antidepressant and antianxiety drugs[6–8] while MAO-B inhibitors have been found to be useful as coadjuvants in the treatment of Parkinson's disease (PD) and Alzheimer's disease (AD).[9–11]

A recent description of the crystal structure of the two isoforms of human MAO by Binda et al. provides a better understanding of the pharmacophoric requirements needed for the rational design of potent and selective enzyme inhibitors.[12–17]

It was reported that numerous compounds among the great variety of substituted hydrazines behave as MAO inhibitors[18–20] and a common structural feature of substrates and inhibitors is an amino or imino group playing in interaction at the active site of the enzyme.[21] 2-Pyrazolines can also be considered as a cyclic hydrazine moiety. For this reason, researchers have investigated MAO and other amine oxidase inhibition activities of 2-pyrazolines and found high activity (Fig. 1).[22–31]

The discovery of this class of drugs has led to a considerable increase in modern drug development and also pointed out the unpredictability of biological activity arising from structural modifications of a prototype drug molecule.

In light of the aforementioned findings, in order to increase our knowledge of the MAO inhibitory activity and selectivity of hydrazine-containing compounds, and to continue our study of pyrazoline derivatives as inhibitors of MAO-A and MAO-B isoforms, we reported here the synthesis and the evaluation of the MAO-A and MAO-B inhibitor activity of the hexahydroindazol derivatives (**1a–2e**). Furthermore, molecular modeling work was performed utilizing docking techniques to explain the selective inhibitory activity toward the MAO-A and MAO-B enzymes.

2. Results and discussion

Our initial goal in this study was to prepare the N-substituted hexahydroindazoles derivatives (Scheme 1), evaluate their monoamine oxidase (MAO) A and B inhibitory activity and carry out docking studies.

2.1. Chemistry

The arylidenecyclohexanones (**1,2**) were synthesized by methods found in the literature.[32,33] The reaction of arylidenecyclohexanone with hydrazine and subsequent isothiocyanate derivatives yielded 2-substituted thiocarbamoyl-3,3a,4,5,6,7-hexahydro-2*H*-indazoles (compounds **1b–1e**, **2b–2e**) while the condensation of arylidenecyclohexanone with thiosemicarbazide was ascribed to 2-thiocarbamoyl-2,3,4,5,6,7-hexahydro-1*H*-indazole derivatives (compounds **1a**, **2a**). These reactions were probably involved in the intermediate formation of hydrazones and subsequent addition of N–H on the olefinic bond of the ethylenic moiety (Scheme 1).

The formation of this bicycle in the course of the addition reaction of arylidenecyclohexanones with hydrazine derivatives resulted in the formation of two stereoisomers: namely, the *cis* isomer (compounds **1b–1d**, **2b–2d**), and the *trans* isomer (compounds **1e**) which is an isomer that had been separated by crystallization from methanol. If the addition reaction is preceded by *trans* addition to the double band, the ring closure of the phenylhydrazone gives rise to the *cis* isomer (**1b–1d**, **2b–2d**). If addition occurs at the opposite side, the *trans* isomer is obtained (**1e**).

However, we were unable to separate the isomers of compound **2e** owing to its close R_f values although compound **2e** after the work up was seen as two spots which were not equal in intensity. We performed crystallization, preparative chromatography and column chromatography many times in order to separate it, but we were not successful. On the other hand, we have concluded that *trans* isomer might be dominant in the diastereomeric mixture from integral values obtained in ^{1}H NMR where the ratio of the heights of the *cis*/*trans* isomers was 0.13/1. Hence, because of the failure to separate the mixture, analytical and spectroscopical measurements in this case have been performed on the mixture as it is.

The structure of the compounds was elucidated by IR, ^{1}H NMR, ^{13}C NMR, DEPT, ^{2}D NMR and EI-MASS techniques.

UV and IR spectra do not serve to distinguish between *cis* and *trans* isomers of 2-thiocarbamoyl-3,3a,4,5,6,7-hexahydro-2*H*-indazoles derivatives. We have turned to NMR to provide additional support for structure assignments based on chemical evidence. Chemical shift and proton coupling constant differences have been observed for *cis*/*trans* isomer pairs in olefins and cyclic compounds and have been used in structure assignments. The ^{1}H NMR spectra of compounds **1b–1d**, **2b–2d** display the signals from vicinal protons at C-3 and C-3a (δ 5.8–6.1 and 3–3.40 ppm, respectively) with J = 10.8–11.2 Hz, which are indicative of their *cis* configuration. In

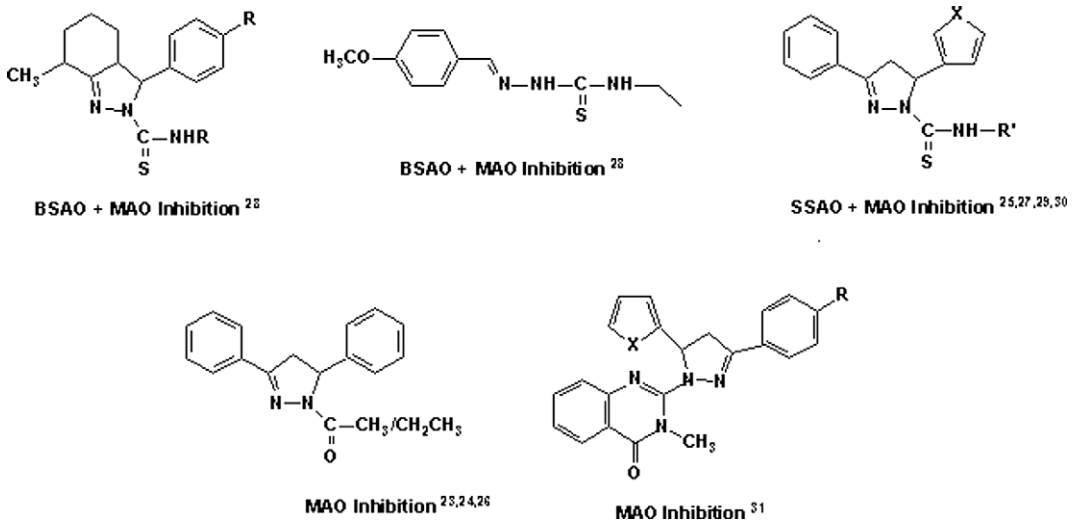

Figure 1. Pyrazole derivatives having MAO, SSAO and BSAO inhibition.

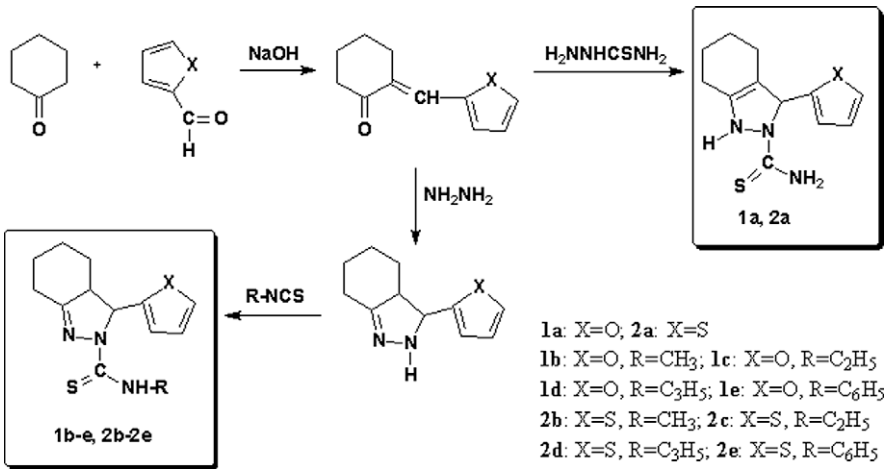

Scheme 1. Synthetic pathway of compounds **la–2e.**

compound **1e**, H-3 and H-3a protons resonated 5.41–5.65 and 3.05–3.12 ppm with J = 4.8–5.2 Hz predicating its *trans* configuration. In the ^{1}H NMR spectrum, the proton at C-3 and the proton on the ring nitrogen and hydrogen atoms attached to the nitrogen atom in the thiocarbamoyl moiety resonated at 8.69–9.97 and 6.45–8.21 ppm, respectively. Chemical shifts of the cyclohexane ring protons also showed characteristic differences in *cis* and *trans* isomers, such that the H-4*ax* proton shifted to a considerably higher field (0.53–0.85 ppm) in *cis* isomers due to the shielding effect of the 3-aryl ring which is oriented close to this proton, while in the *trans* isomer it overlapped with H-5*ax* and H-6*ax* protons in the range 1.4–1.6 ppm. The protons belonging to the aromatic ring and the other aliphatic groups were observed with the expected chemical shift and integral values. All compounds gave satisfactory elemental analyses.

In the ^{13}C NMR of the *cis* isomer, the thiophen ring attached to C-3 and H-4*ax* appeared to have steric interactions, as was evident from the lower values of the chemical shifts for C-4 for the *cis*- than for the *trans* isomer of the compound **1e** with the furan ring attached to C-3. In the DEPT spectra of compound **1a**, four methylene and four methine carbons were seen in expected values. For the complete assignment of all protons, two dimensional NMR techniques (^{1}H–^{1}H-COSY and ^{13}C–^{1}H COSY) were utilized.

Inspection of the ^{1}H–^{13}C NMR spectrum of compound **1a** revealed a correlation from signal at 2.43 and 2.77 ppm to signal at 27 and 29 ppm of C-4/C-7 and vice versa. But which signal was H-7 or H-4 was unknown. Because of this, we utilized ^{1}H–^{1}H COSY spectrum for understanding which of the signal at 2.43 or 2.77 ppm belong to H-4 or H-7 protons. The correlation between the signal of H-3 (6.45–6.48 ppm)/H-3′,4′,5′ (6.45–6.48/6.45–6.48/7.47 ppm) and the signal at 2.43 ppm confirmed that that signal (at 2.43 ppm) corresponded to axial and equatorial protons of H-4. Therefore, the other signal at 2.77 ppm could be assigned the axial and equatorial protons of H-7.

In the mass spectra, molecular ion signals were prominent for all compounds for which six of them were also base signal (compounds **1a–1e**, **2c**). Two sets of fragments were detected belonging to the fragmentation of the thiocarbamoyl and bicyclic dihydropyrazole structure. Fragments resulting from the loss of an SH ion from the thiocarbamoyl group were observed for most compounds in different intensity (compounds **1a**, **2a–e**). In addition to, α-cleavage of the C=S group in both sides causing ejection of the NHR (compounds **1d**, **2d**) or CSNHR (compounds **1a, 1b, 2a, 2e**) type of ions were also observed.

The X-ray diffraction data of the crystal obtained for compound **1e** showed that compound **1e** is in the *trans* configuration (Fig. 2).

2.2. X-ray crystal analysis of compound 1e

The molecular structure of compound **1e** was determined by X-ray crystallographic analysis. The compound crystallizes in the tetragonal system, space group $P4_1$ with a = 10.600(2) Å, b = 10.600(2) Å, c = 14.863(4) Å, α = 90.00°, β = 90.00°, γ = 90.00°. Ortep depiction with atom numbering of compound **1e** is shown in Figure 2.

The S1–C8 and N1–C7A bond lengths are both indicative of a significant double bond character (Table 1). All the C–C bond distances in the benzene ring have typical Csp^2–Csp^2 values. The average C–C bond distance within benzene ring is 1.370(2) Å. The C10–N9–C8–N2 torsion angle is 177.7(8)°.

The furan and benzene rings are planar, the maximum deviations from the least-squares planes being 0.0063(3) Å for atom C5′ and 0.0072(2) Å for atom C15. The dihedral angles are as follows: 84.74(2)° between furan and N2–N1–C7A–C3A–C3 ring and 43.07(3)° between benzene and furan rings.

The hexahydroindazol ring exhibits a puckered conformation, with puckering parameters[33] q_2 = 0.069 (10) Å, q_3 = 0.537 (10) Å, Q_T = 0.541 (10) Å, φ = 224 (8)° and θ = 7.0 (11)°, which indicates that the hexahydroindazol ring has a chair conformation. The largest deviations from the best plane are −0.253 (2) Å for C4 and 0.254 (2) Å for C5. The hexahydroindazol ring makes a dihedral angle of 37.22 (3)° with the N2–N1–C7A–C3A–C3 ring. It has also been found that the H3A and H3 atoms deviate from the latter plane in opposite directions. The magnitudes of the deviations of H3A and H3 atoms in opposite directions are equal to 0.39 Å and 0.4 Å, respectively, constituting a *trans* configuration.

2.3. Biochemistry

MAO-A and MAO-B inhibitory activities of newly synthesized hexahydroindazole derivatives were determined using MAO-A and -B isoforms of rat liver mitochondrial pellets. Liver tissue was used to screen the MAO-inhibitory actions of these novel compounds since liver was reported to be a good source for both isoforms of the enzyme. According to the IC_{50} values corresponding to the inhibition of rat liver MAO by the newly synthesized hexahydroindazole derivatives, all of the compounds were found to inhibit rat liver MAO. All novel compounds were reversible inhibitors of rat liver MAO since the enzyme activity (approx. 98–100%) was restored after 24 h dialysis (Table 2).

The thiosemicarbazide moiety in the parent structure was suggested to be responsible for the MAO inhibitory activity of the newly synthesized compounds. According to our experimental

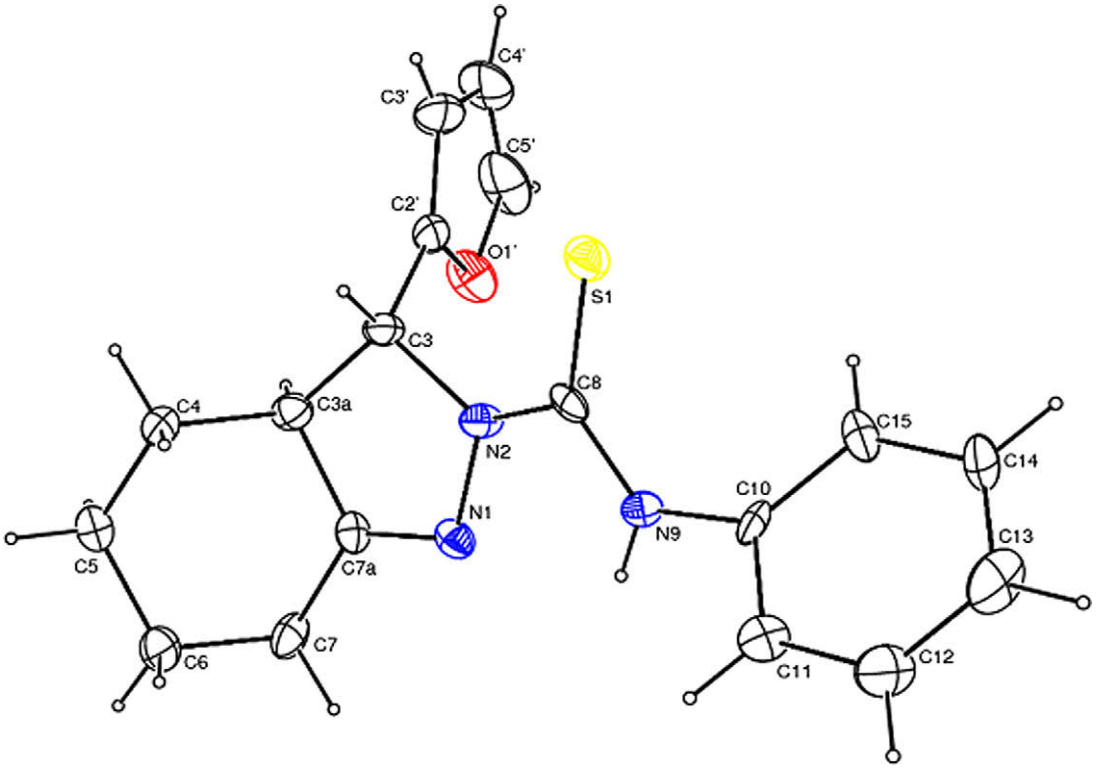

Figure 2. The molecular structure of **Ie**, showing the atom-numbering scheme. Displacement ellipsoids are drawn at the 40% probability.

Table 1
Selected geometric parameters (Å) and crystallographic parameters for the compound **1e**

Selected bond lengths (Å)		Crystallographic parameters for the compound **1e**	
C1–N1	1.430(10)	Chemical formula sum	$C_{18}H_{19}N_3OS$
N1–C7	1.355(10)	Chemical formula weight	325.42
N2–N3	1.400(8)	Symmetry cell setting	Tetragonal
N2–C14	1.500(9)	Space group	$P4_1$
S1–C7	1.666(9)	*a* (Å)	10.600(2)
C7–N2	1.35(1)	*b* (Å)	10.600(2)
N3–C8	1.277(9)	*c* (Å)	14.863(4)
		α (°)	90.00
		β (°)	90.00
		γ (°)	90.00

data, compounds **1d** (*cis*), **1e** (*trans*), **2c** (*cis*), **2d** (*cis*) and **2e** (*mixture*) inhibited MAO-A while **1a** (*cis*), **1b** (*cis*), **1c** (*cis*), **2a** and **2b** (*cis*) inhibited MAO-B selectively. The mode of inhibition was found to be competitive and reversible for all compounds tested.

Since IC_{50} value for a compound is generally calculated from the experiments which a wide range of inhibitor concentration used in, and this value cannot give an idea about the kinetic behavior of the inhibitor, we preferred to discuss the data upon K_i values. In respect to the K_i values experimentally found (Table 2), compounds **1e** [3-(2-furyl)-2-(*N*-phenylthiocar-bomoyl)-3,3a,4,5,6,7-hexahydro-*2H*-indazole] and **2e** [3-(2-thienyl)-2-(*N*-phenylthiocarba-moyl)-3,3a,4,5,6,7-hexahydro-*2H*-indazole], which carry a phenyl substituent on the nitrogen atom were found to be highly

Table 2
Experimental IC_{50} and K_i values corresponding to the inhibition of rat liver MAO isoforms by the newly synthesized hexahydroindazole derivatives[a]

Compounds	IC_{50} for MAO-A[b] (μM)	K_i value for MAO-A[b]	IC_{50} for MAO-B[b] (μM)	K_i value for MAO-B[b]	Inhibition type	Reversibility	SI[c] MAO-A/MAO-B	MAO inhibitory selectivity
1a	80.22 ± 6.91	3.90 ± 0.28 μM	1.37 ± 0.10	0.96 ± 0.01 nM	Competitive	Reversible	4062.50	Selective for MAO-B
1b	108.34 ± 7.09	8.82 ± 0.61 μM	2.99 ± 0.15	2.10 ± 0.01 μM	Competitive	Reversible	4.20	Selective for MAO-B
1c	110.45 ± 8.56	4.26 ± 0.30 μM	2.77 ± 0.96	1.95 ± 0.05 μM	Competitive	Reversible	2.19	Selective for MAO-B
1d	1.78 ± 0.17	0.65 ± 0.03 μM	113.88 ± 9.70	4.05 ± 0.28 μM	Competitive	Reversible	0.16	Selective for MAO-A
1e	0.78 ± 0.08	4.22 ± 0.33 nM	80.45 ± 7.45	1.23 ± 0.01 μM	Competitive	Reversible	0.0034	Selective for MAO-A
2a	95.20 ± 6.89	2.99 ± 0.17 μM	1.26 ± 0.01	0.90 ± 0.01 nM	Competitive	Reversible	3322.22	Selective for MAO-B
2b	62.34 ± 5.10	5.01 ± 0.38 μM	2.61 ± 0.18	1.69 ± 0.09 μM	Competitive	Reversible	2.96	Selective for MAO-B
2c	3.01 ± 0.29	1.72 ± 0.01 μM	90.12 ± 8.72	3.01 ± 0.23 μM	Competitive	Reversible	0.57	Selective for MAO-A
2d	2.05 ± 0.17	0.88 ± 0.01 μM	78.62 ± 5.03	2.90 ± 0.17 μM	Competitive	Reversible	0.30	Selective for MAO-A
2e	0.70 ± 0.02	39.15 ± 2.70 nM	75.12 ± 5.87	92.26 ± 7.13 μM	Competitive	Reversible	0.004	Selective for MAO-A
Selegiline	90.55 ± 7.05	105.66 ± 9.21 μM	1.60 ± 0.10	1.35 ± 0.12 μM	Competitive	Reversible	78.26	Selective for MAO-B
Moclobemide	5.70 ± 0.37	5.53 ± 0.27 nM	89.55 ± 6.30	1.08 ± 3.00 μM	Competitive	Reversible	0.005	Selective for MAO-A

[a] Each value represents the mean ± SEM of three independent experiments.
[b] IC_{50} and K_i values were determined from the kinetic experiments in which *p*-tyramine (substrate) was used at 500 μM to measure MAO-A and 2.5 mM to measure MAO-B. Pargyline or clorgyline were added at 0.50 μM to determine the isoenzymes A and B. Newly synthesized compounds and the known inhibitors were preincubated with the homoganates for 60 min at 37 °C.
[c] Selectivity index. It was calculated as K_i (MAO-A)/K_i (MAO-B).

potent MAO-A inhibitors. These two molecules differ from each other with the existence of furyl or thienyl groups at the 3-position of the hexahydroindazole ring. MAO-A/MAO-B selectivities of compound **1e** (bearing a furyl group) and **2e** (bearing a thienyl group) were found be 0.0034 and 0.004, respectively, while MAO-A/MAO-B selectivity of moclobemide, the known selective MAO-A inhibitor, was calculated as 0.005. Since the *trans* and *cis* forms of compound **2e** could not be separated following the synthesis, experimental inhibition studies were conducted only with the mixture obtained.

According to the experimental findings, compound **1e** was found to inhibit rat liver MAO-A potently and selectively with a K_i value of 4.22 ± 0.33 nM. Compound **2e** also inhibited rat liver MAO-A potently. The K_i values corresponding to the inhibition of rat liver MAO-A with compound **2e** were calculated as 20.95 nM and 31.17 μM for its *trans* and *cis* configurations (Table 3), respectively, from the docking studies. Thus, this cross tabulation and the integration values obtained in ^{1}H NMR support the hypothesis that the compound **2e** might be mainly in *trans* configuration. Since compounds **1e** and **2e**, which bear a phenyl group on thiosemicarbazide moiety appeared as potent MAO-A inhibitors (experimental and calculated K_i values are in nM range), it was suggested that phenyl substitution increases the MAO-A inhibitory potency of the derivatives studied.

Compounds **1d** and **2d** which contain an allyl derivative on the nitrogen atom also inhibited rat liver MAO-A selectively and reversibly in a competitive manner. These two molecules also differ from each other with respect to furyl and thienyl groups at the hexahydroindazole ring. Although the MAO-A/MAO-B selectivities of compounds **1d** and **2d** were calculated from the experimental data as 0.16 and 0.30, and as 0.15 and 0.13, from the docking studies, respectively. These two compounds therefore are also potent MAO-A inhibitors among the novel compounds studied in respect to both calculated and experimental data (Table 3).

Compound **1c** carrying an ethyl group on the nitrogen atom and a furyl group on the hexahydroindazole ring inhibited rat liver MAO-B while compound **2c** carrying a thienyl group instead of furyl inhibited rat liver MAO-A selectively and reversibly in a competitive manner.

Compounds **1a** and **1b** bearing non-substituted or *N*-methylthiocarbamoyl and a furyl group on the hexahydroindazole ring inhibited rat liver MAO-B potently as compounds **2a** and **2b**, the thienyl bearing ones. Compound **1a** appeared as the most potent compound in this group. Its experimental SI (MAO-B/MAO-A) was calculated as 2.46. Compound **2a** was found to be the most potent MAO-B inhibitor with an experimental K_i value of 0.90 ± 0.01 nM. This new compound inhibited rat liver MAO-B more potently than selegiline (K_i value was determined as 1.35 ± 0.12 μM), the well known MAO-B inhibitor (Fig. 3).

Among all novel derivatives studied, compound **1e** was found to be the most potent MAO-A inhibitor with an experimental K_i value of 4.22 ± 0.33 nM. This new compound was more potent than moclobemide, the well known MAO-A inhibitor (K_i value was determined as 5.53 ± .0.27).

The results presented here show that newly synthesized hexahydroindazole derivatives may be promising candidates as potent anti-depressant/anti-parkinson agents. At the same time, this study indicates a significant correlation between the docking results and experimental ones. However, further experiments are necessary to fully elucidate the binding characteristics of the novel compounds to MAO isoforms purified from different sources since it was recently shown that the similarities and differences between human MAO-A (hMAO-A) and rat MAO-A (rMAO-A) might be important in drug development.[34] Although these two enzymes exhibit ~90% sequence identity, they reveal significant differences in their quaternary structures. The volume of the active site cavity of rMAO-A (~450 Å) is smaller than that of hMAO-A (~550 Å). It should be kept in mind that the results obtained with non-human forms of MAO (e.g., the evaluation of the inhibitory properties of a compound) may not be extrapolated to the same situation in humans.[35]

2.4. Molecular docking studies

Compound **1a** is docked in the active site of the MAO-A enzyme as shown in Figure 4 (K_i = 1.36 μM). When examined closely, it is observable that the furane ring is oriented horizontally between the phenolic side chains of Tyr444 and Tyr407 residues and it is approaching from the *re* face of FAD. The hydrogen atom on the amine group on the side chain makes a hydrogen bond with the backbone carbonyl group of Ile180 (2.16 Å). Ile207, Asn181 and Tyr197 are the other active site residues interacting with the inhibitor. The same compound shows different binding patterns with the MAO-B enzyme as shown in Figure 5 (K_i = 1.27 μM). The inhibitor is placed far distant from the hydrophobic cage surrounded by Tyr398, Tyr435 and FAD. In this case the inhibitor is located close to the entrance cavity. One of the thiocarbamoyl hydrogens of the inhibitor makes a hydrogen bond with the entrance site residue

Table 3
Calculated and experimental K_i values corresponding to the inhibition of MAO isoforms by the newly synthesized hexahydroindazole derivatives[a]

Compound	Calculated K_i values for MAO-A[a]	Experimental K_i values for MAO-A[b]	Calculated K_i values for MAO-B[a]	Experimental K_i values for MAO-B[b]	Calculated SI[c] MAO-A/MAO-B	Experimental SI[c] MAO-A/MAO-B	Selectivity
1a	1.36 μM	3.90 ± 0.28 μM	1.27 μM	0.96 ± 0.01 nM	1.07	4062.50	Selective for MAO-B
1b	3.18 μM	8.82 ± 0.61 μM	2.90 μM	2.10 ± 0.01 μM	1.09	4.20	Selective for MAO-B
1c	2.80 μM	4.26 ± 0.30 μM	2.73 μM	1.95 ± 0.05 μM	1.02	2.19	Selective for MAO-B
1d	0.525 μM	0.65 ± 0.03 μM	3.58 μM	4.05 ± 0.28 μM	0.14	0.16	Selective for MAO-A
1e	8.77 nM	4.22 ± 0.33 nM	70.72 nM	1.23 ± 0.01 μM	0.12	0.0034	Selective for MAO-A
2a	2.07 μM	2.99 ± 0.17 μM	1.11 μM	0.90 ± 0.01 nM	1.86	3322.22	Selective for MAO-B
2b	2.62 μM	5.01 ± 0.38 μM	1.70 μM	1.69 ± 0.09 μM	1.54	2.96	Selective for MAO-B
2c	0.422 μM	1.72 ± 0.01 μM	2.47 μM	3.01 ± 0.23 μM	0.17	0.57	Selective for MAO-A
2d	0.268 μM	0.88 ± 0.01 μM	1.99 μM	2.90 ± 0.17 μM	0.13	0.30	Selective for MAO-A
2e *trans*	20.95 nM	39.15 ± 2.70 nM	69.46 nM	92.26 ± 7.13 μM	0.3	0.004	Selective for MAO-A
2e *cis*	31.17 μM	—	93.08 nM	—	340.5	—	Selective for MAO-B
Selegiline	—	105.66 ± 9.21 μM	—	1.35 ± 0.12 μM	—	78.26	Selective for MAO-B
Moclobemide	—	5.53 ± 0.27 nM	—	1.08 ± 3.00 μM	—	0.005	Selective for MAO-A

[a] K_i values were determined from the kinetic experiments in which *p*-tyramine (substrate) was used at 500 μM to measure MAO-A and 2.5 mM to measure MAO-B. Pargyline or clorgyline were added at 0.50 μM to determine the isoenzymes A and B. Newly synthesized compounds and the known inhibitors were preincubated with the homoganates for 60 min at 37 °C.
[b] Each value represents the mean ± SEM of three independent experiments.
[c] Selectivity index. It was calculated as K_i (MAO-A)/K_i (MAO-B).

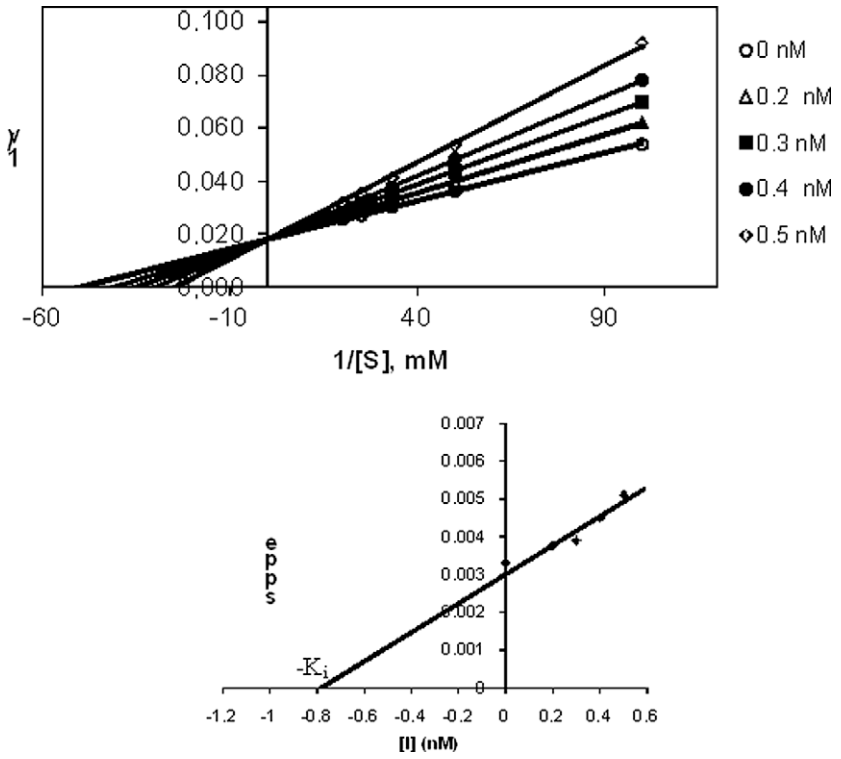

Figure 3. Lineweaver–Burk plot for the inhibition of rat liver MAO-B by the compound **2a** (0–0.5 nM) with 60 min of preincubation at 37 °C. *p*-Tyramine was used as substrate (0.01–0. l mM). Values are the mean of three independent experiments. Second graph represents the plot of the slope of reciprocal plot, *v* = velocity (nmol/saat/mg).

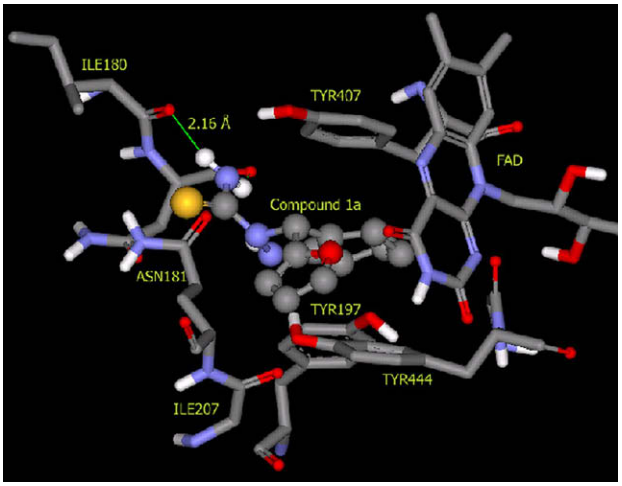

Figure 4. Binding mode of compound **Ia** in MAO-A active site.

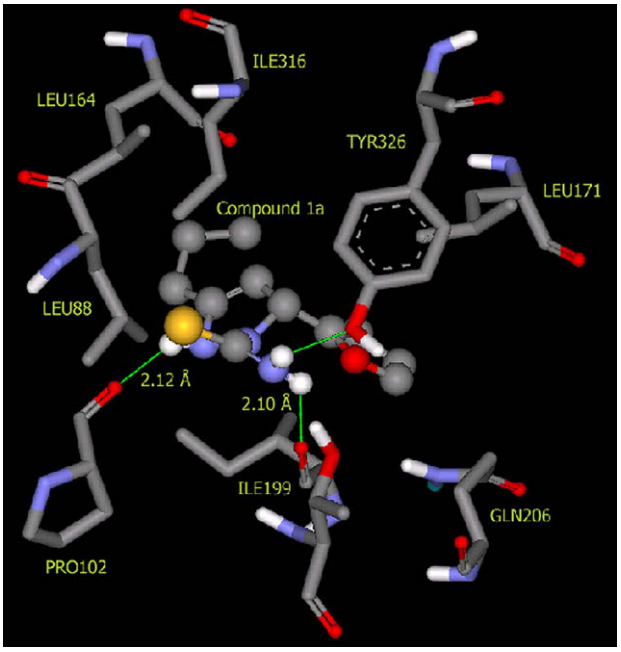

Figure 5. Binding mode of compound **Ia** in MAO-B active site.

Ile199 (2.10 Å). The second hydrogen bond forms between Pro102 backbone carbonyl group and amine hydrogen of the indazole ring. Leu88, Gln206, Tyr326, Ile316, Leu164 and Leu171 are the other residues stabilizing the inhibitor tightly at this volume.

Figure 6 shows the binding pose of **1d** in the active site of MAO-A. The *N*-allylthiocarbamoyl moiety of compound **1d** is sandwiched between Tyr407 and Tyr444 and it approaches to FAD as closely as possible (K_i = 0.525 μM). In addition, the N-H group of the thiocarbamoyl moiety and OH group of the Tyr407 makes a strong hydrogen bond (1.96 Å). Asn181, Phe208, Ile207 and Glu216, Ile180 and Ser209 side chains are the other residues interacting with the inhibitor in the active site of the MAO-A. On the other hand **1d** is oriented differently in the active site of MAO-B than that of MAO-A in Figure 7 (K_i = 3.58 μM). None of the groups of the ligand is sandwiched between Tyr435 and Tyr398 and it is not as close to FAD as in MAO-A, causing a low potency (K_i = 3.58 μM) when compared with MAO-A (K_i = 0.525 μM). The major contribution of binding energy comes from the hydrogen bond resulting from the Tyr326 side chain OH and thiocarbamoyl hydrogen (2.05 Å). The other contributing van der Waals interactions are between

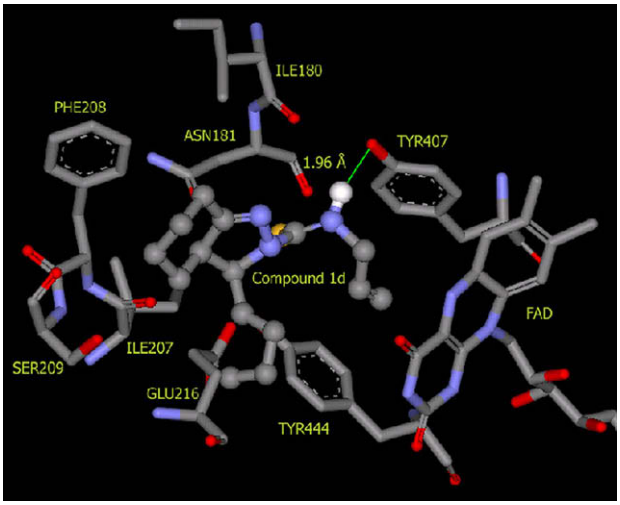

Figure 6. Binding mode of compound **Id** in MAO-A active site.

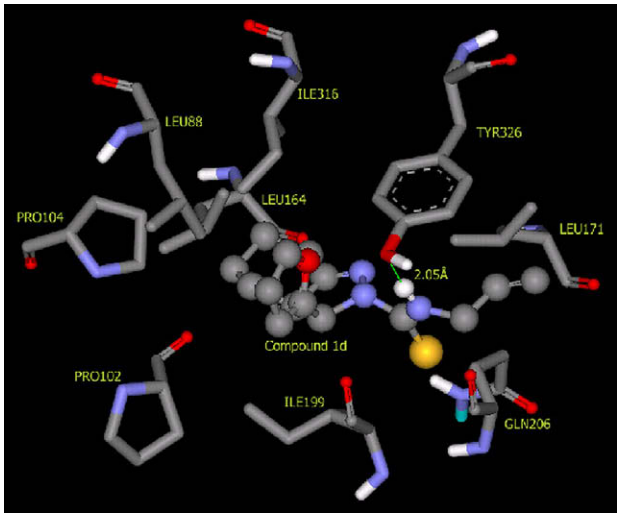

Figure 7. Binding mode of compound **Id** in MAO-B active site.

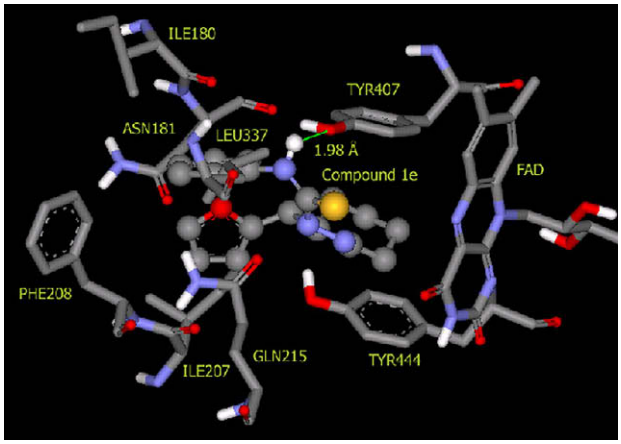

Figure 8. Binding pose of compound **Ie** in the active site ofMAO-A.

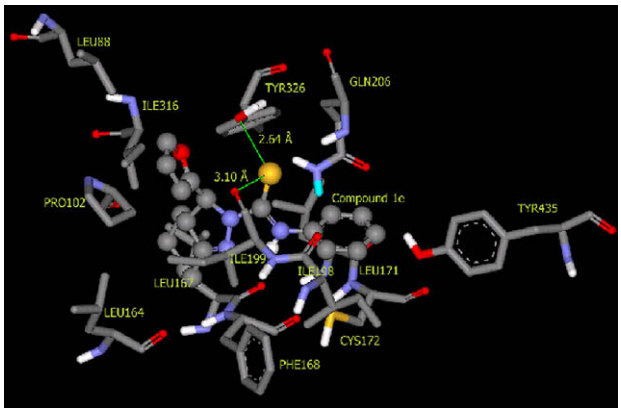

Figure 9. Binding pose of compound **Ie** in the active site of MAO-B.

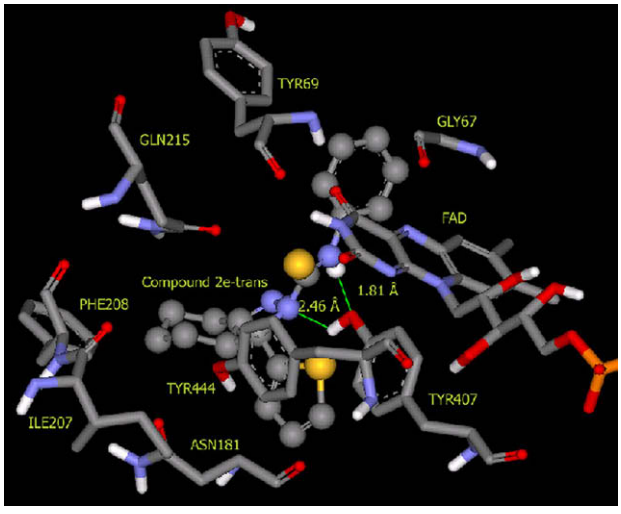

Figure 10. Binding mode of compound **2e**-*trans* in MAO-A active site.

the residues of Leu88, Ile316, Pro104, Pro102, Ile199, Leu164 and Gln206.

Figure 8 shows the compound **1e** in the active site of MAO-A (K_i = 8.77 nM). The hexahydo-1*H*-indazole ring of compound **1e** is approached to FAD as close as possible and perfectly sandwiched between Tyr407 and Tyr444. In addition to that, hydrogen atom of the N–H group is making an excellent hydrogen bond with the O–H group of Tyr407 (1.98 Å) in the hydrophobic cage. Ile180, Asn181, Leu337, Phe208, Ile207 and Gln215 are the other residues having very close contact with the inhibitor. This compound has the lowest inhibition constant value among the compounds calculated computationally. In the MAO-B complex of the same compound, inhibitor occupies a volume far from FAD ring (K_i = 70.72 nM). The phenyl ring is oriented toward Tyr435 and surrounded by Gln206, Cys172, Ile198 and Gln206. Sulfur atom of the thioamide moiety group is making two close interaction; one with the backbone carbonyl group of Ile199 and the other with the hydroxyl group of Tyr326. The hexahydo-1*H*-indazole ring is, on the other hand, surrounded by Leu88, Ile316, Pro102, Leu167, Leu164 and Phe168 (Fig. 9).

In Figure 10 the compound **2e**-*trans* is shown (K_i = 20.95 nM). In the complex of MAO-A with the *trans* isomer of compound **2e**, the thiophene ring is snugly sandwiched between Tyr407, Tyr444 in the hydrophobic package vertically to the *re* face of FAD. The phenyl ring is placed between Glu 216 and Phe 208 at the entrance cavity. There is one close interaction between the Tyr407 side chain and benzylic N-H moiety (1.81 Å). Tyr69, Gln215, Phe208, Ile207 and Asn181 are the other residues having close contact with the inhibitor. In the MAO-B complex of the same compound, the

phenyl ring is surrounded by Ile198, Gln206 and Cys172. The cyclohexane ring is, on the other hand, surrounded by Leu167, Leu164 and Ile316. The thiophene ring has neighboring Ile199, Pro102 and Leu88 residues (Fig. 11).

3. Conclusion

The biological behavior of the hexahydroindazol derivatives was investigated against both MAO-A and -B isoforms. Most of them showed potent inhibition activities in the micromolar range with selectivity against the MAO-A and MAO-B isoform. It was determined that the length of the lateral chain of the aryl diazo derivatives should not be longer than two atoms as was observed for the substrates of MAO-B (benzylamine, phenylethylamine). The presence of the longer and volumed groups on thiocarbamoyl nitrogen could be indicated as a requisite for the selective MAO-A activity. The docking studies carried out on the most active and selective compounds **1a**, **1d**, **1e and 2e**-*trans* provided us new and complementary insights into the inhibition mechanism and patterns. These results encouraged us to pursue our molecular modeling studies in designing more potent/selective MAO inhibitors based on the hexahydroindazole scaffold.

4. Experimental

4.1. Chemistry

All chemicals were obtained from Merck Co. except 2-furaldehyde. 2-Furaldehyde was obtained from Sigma–Aldrich Co. Melting points were determined through a Thomas Hoover capillary melting point apparatus and are uncorrected. Ultraviolet (UV) spectra were recorded with an Agilent 8453 UV–vis spectra spectrometer in methanol approximately 4×10^{-5} M concentration. Infrared (IR) spectra were obtained with a Perkin Elmer Spectrum BX FT-IR spectrometer using potassium bromide plates and the results were expressed in wave number (cm^{-1}). Nuclear magnetic resonance (^1H NMR and ^{13}C NMR) spectra were scanned on a Varian 400 and 100 MHz High Performance spectrometer, respectively, using dimethylsulfoxide (DMSO-d_6) as a solvent. Chemical shifts are expressed in δ (parts per million) relative to tetramethylsilane. Splitting patterns are as follows: s, singlet; d, doublet; t, triplet; m, multiplet; dq, doublet of quartet; dt, doublet of triplet; sb, singlet broad. The mass spectra were obtained with electron impact technique using a Direct Insertion Probe and Agilent 5973-Network Mass Selective Dedector at 70 eV. Elemental analyses (C, H, N, S) were performed on a Leco CHNS 932 analyzer.

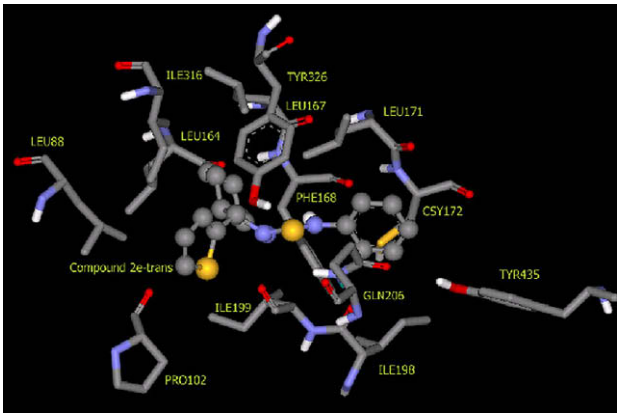

Figure 11. Binding mode of compound **2e**-*trans* in MAO-B active site.

4.1.1. Synthesis of 2-furfurylidene/2-(2-thienylmethylene)cyclohexanone

2-Furfurylidene/2-(2-thienylmethylene)cyclohexanone was synthesized as a result of the reaction of cyclohexanone and furfural/thiophene-2-aldehyde in basic media with 1 N NaOH at room temperature according to the method reported earlier.[36]

4.1.2. General procedure for the preparation of 3-(2-furyl/thienyl)-2-thiocarbamoyl-1,3,4,5,6,7-hexahydro-1*H*-indazoles (1a, 2a)

One gram (0.025 mol) NaOH in 5 ml water was added to 0.01 mol of 2-furfurylidene/2-(2-thienylmethylene)cyclohexanone and 1.092 g (0.012 mol) thiosemicarbazide. The reaction mixture was refluxed for 8 h than poured into 200 ml of cold water. The precipitate was filtered and recrystallized from methanol.

4.1.3. General procedure for the preparation of 3-(2-furyl/thienyl)-2-(*N*-substitued thiocarbamoyl)-3,3a,4,5,6,7-hexahydro-2*H*-indazoles (1b–e, 2b–e)

One gram (0.02 mol) hydrazine hydrate (100%) was added to 0.01 mol of 2-furfurylidene/2-(2-thienylmethylene)cyclohexanone in 20 ml ethanol and refluxed for 2 h. Reaction mixture was cooled and solvent evaporated under vacuum. The intermediate 3-(2-furyl/thienyl)-3,3a,4,5,6,7-hexahydro-2*H*-indazole was solved in 20 ml dry ether. 0.01 mol appropriate isothiocyanate and four drops of triethylamine was added into this solution and the reaction mixture was mixed for 4 h at room temperature. The precipitate was filtered and recrystallized from appropriate solvents.

4.1.3.1. 3-(2-Furyl)-2-thiocarbamoyl-2,3,4,5,6,7-hexahydro-1*H*-indazol (1a). A dark yellow solid substance with a yield of 54% and recrystallized from methanol. Mp 184–5 °C. *UV* (CH_3OH) nm: 202 (log ε: 4.24) and 3 nm. (log ε: 4.32); *IR* (KBr) cm^{-1}, 34, 3211, 3130, 3035, 29, 2864, 1595, 1497, 1261, 1151, 1080; ^1H NMR (DMSO-d_6, 400 MHz) δ (ppm): 1.59–1.64 (4H; m; $H_{5ax,}$ $H_{5eq,}$ $H_{6ax,}$ H_{6eq}), 2.50 (2H; m; H_{4ax}, H_{4eq}), 2.68 (2H; t; H_{7ax}, H_{7eq}), 6.58 (2H; m; furan $H_{3,}$ furan H_4), 7.21 (1H; m; H_3), 7.74 (1H; d; furan H_5), 7.85 and 8.21 (1H; s; NH_2), 9.97 (1H; s; H_1); ^1H NMR ($CDCl_3$, 400 MHz) δ (ppm): 1.69–1.80 (4H; m; $H_{5ax,}$ $H_{5eq,}$ $H_{6ax,}$ H_{6eq}), 2.43 (2H; t; H_{4ax}, H_{4eq}), 2.77 (2H; dt; H_{7ax}, H_{7eq}), 6.45–6.48 (3H; m; furan $H_{3,}$ furan H_4, NH_2), 7.05 (1H; m; H_3), 7.26 (1H; s; NH_2), 7.46 (1H; d; furan H_5), 8.69 (1H; s; H_1); ^{13}C NMR (400 mHz, DMSO-d_6) δ (ppm); 22 (C_5), 23 (C_6), 27 (C_4), 29 (C_7), 112 (furan-C_3, furan-C_4), 116 (C_3), 133 (C_{3a}), 144 (furan-C_5), 151 (C_{7a}), 153 (furan-C_2), 179 (C=S); ^{13}C NMR (400 mHz, $CDCl_3$) δ (ppm); 22 (C_5), 23 (C_6), 27 (C_4), 29 (C_7), 112 (furan-C_3, furan-C_4), 117 (C_3), 132 (C_{3a}), 143 (furan-C_5), 152 (C_{7a}), 153 (furan-C_2), 179 (C=S); *HSQC* (^1H–^{13}C NMR)($CDCl_3$); 1.69–1.180/22 (H_{5ax}, H_{5eq}/C_5), 1.69–1.180/23 (H_{6ax}, H_{6eq}/C_6), 2.43/27 (H_{4ax}, $H_{4eq,}$/C_4), 2.68/29 (H_{7ax}, H_{7eq}/C_7), 7.05/117 (H_3/C_3), 6.45–6.48/112 (furan H_3/furan C_3), 6.45–6.48/112 (furan H_4/furan C_4), 7,46/143 (furan H_5/furan C_5); *MS* (70 eV, EI): *m*/*e* (%) 249: (M^+, 100%), 216 (M−SH, %18.), 189 (M−$CSNH_2$, %67.82), 181 (M−C_4H_4O;%15.78), 161 (M−CH_2N_3S, %31.57). Anal. Calcd for $C_{12}H_{15}N_3OS$: C, 57.81; H, 6.06; N, 16.85; S, 12.86. Found: C, 57.71; H, 6,181; N, 16.; S, 12.64.

4.1.3.2. 3-(2-Furyl)-2-(*N*-methylthiocarbamoyl)-3,3a,4,5,6,7-hexahydro-2*H*-indazol (1b). A dirty white solid substance with a yield of 31% and recrystallized from methanol–water. Mp 167–8 °C. *UV* (CH_3OH) nm: 201 (log ε: 4.36) and 273 nm. (log ε: 4.31); *IR* (KBr) cm^{-1}; 3345, 3112, 2987, 2953, 2864, 1649, 1535, 1322, 1216, 1144,1106; ^1H NMR (DMSO-d_6, 400 MHz) δ (ppm) (J in Hz): 0.55 (1H; dq; H_{4ax}), 1.10–1.40 (2H; m; H_{5ax}, H_{6ax}), 1.66 (2H; m; $H_{4eq,}$ H_{5eq}), 1.92 (1H; m; H_{6eq}), 2.26 (1H; dt; H_{7ax}), 2.58 (1H; d; H_{7eq}), 2.86 (3H; d; $-CH_3$), 3.40 (1H; m; H_{3a}), 5.80 (1H; d; H_3; *J*: 10.8), 6.08 (1H; d; furan H_4), 6.35 (1H; dd; furan H_3), 7.51 (1H;

m; furan H_5), 8.12 (1H; q; NH); **MS** (70 eV, EI): *m*/*e* (%): 263 (M^+, 100%), 195 (M−C_4H_4O, %23.68), 189 (M−C_2H_4NS, %17.54), 181 (M−C_6H_{10}, %27.19), 167 (M−$C_6H_{10}N$, %67.82), 107 (M−$C_7H_{12}N_2S$, %14.), 81 (M−$C_8H_{12}N_3S$, %30.70). Anal. Calcd for $C_{13}H_{17}N_3OS$: C, 59.29; H, 6.51; N, 15.96; S, 12.18. Found: C, 59.09; H, 5.68; N, 15.62; S, 11.38.

4.1.3.3. 3-(2-Furyl)-2-(*N*-ethylthiocarbamoyl)-3,3a,4,5,6,7-hexahydro-2*H*-indazol (1c). A white solid substance with a yield of 51% and recrystallized from ethanol. Mp 186 °C. *UV* (CH_3OH) nm: 202 (log ε: 4.34) and 274 nm. (log ε: 4.33); *IR* (KBr) cm^{-1}; 3339, 3110, 2975, 2927, 2862, 1637, 1533, 1323, 1214, 1145, 1112; ^1H NMR (DMSO-d_6, 400 MHz) δ (ppm) (*J* in Hz): 0.53 (1H; dq; H_{4ax}), 1.06 (3H; t; $-CH_3$), 1.10–1.40 (2H; m; H_{5ax}, H_{6ax}), 1.65 (2H; m; H_{4eq}, H_{5eq}), 1.92 (1H; m; H_{6eq}), 2.26 (1H; dt; H_{7ax}), 2.60 (1H; d; H_{7eq}), 3.40 (1H; m; H_{3a}), 3.50 (2H; m; $-CH_2-$), 5.81 (1H; d; H_3; *J*: 10.8), 6.08 (1H; d; furan H_4), 6.35 (1H; dd; furan H_3), 7.51 (1H; m; furan H_5),, 8.10 (1H; t; NH); *MS* (70 eV, EI): *m*/*e* (%): 277 (M^+, 100%), 209 (M−C_4H_4O, %18), 195 (M−C_6H_{10}, %22), 181 (M−$C_6H_{10}N$, %53.47), 107 (M−$C_8H_{14}N_2S$, %15), 81 (M−$C_9H_{14}N_3S$, %31.57), 44 (M−$C_{12}H_{13}N_2OS$, %29). Anal. Calcd for $C_{14}H_{19}N_3OS$: C, 60.62; H, 6.90; N, 15.15; S, 11.56. Found: C, 60; H, 6.97; N, 15.05; S, 10.88.

4.1.3.4. 3-(2-Furyl)-2-(*N*-allylthiocarbamoyl)-3,3a,4,5,6,7-hexahydro-2*H*-indazol (1d). A white solid substance with a yield of 45% and recrystallized from methanol–water. Mp 161 °C. *UV* (CH_3OH) nm: 202 (log ε: 4.32) and 274 nm. (log ε: 4.27); *IR* (KBr) cm^{-1}; 3345, 3112, 2981, 2939, 2863, 16, 1528, 1322, 1217, 1147, 1119; ^1H NMR (DMSO-d_6, 400 MHz) δ (ppm) (*J* in Hz): 0.56 (1H; dq; H_{4ax}), 1.17 (1H; m; H_{5ax}), 1.32 (1H; m; H_{6ax}), 1.67 (2H; m; H_{4eq}, H_{5eq}), 1.92 (1H; m; H_{6eq}), 2.28 (1H; dt; H_{7ax}), 2.60 (1H; d; H_{7eq}), 3. (1H; m; H_{3a}), 4.10 (2H; m; $-CH_2-$), 5.06 (2H; dq; $=CH_2$), 5.80–5.87 (2H; m; $-CH=$, H_3; *J*: 10.8), 6.09 (1H; d; furan H_4), 6.36 (1H; dd; furan H_3), 7.52 (1H; m; furan H_5), 8.19 (1H; t; NH); *MS* (70 eV, EI): *m*/*e* (%): 289 (M^+, 100%), 274 (M−CH_3, %37.72), 233 (M−C_3H_6N, %36), 193 (M−$C_6H_{10}N$, %43), 107 (M−$C_9H_{14}N_2S$, %48.74), 81 (M−$C_{10}H_{14}N_3S$, %63.47). Anal. Calcd for $C_{15}H_{19}N_3OS$: C, 62.25; H, 6.62; N, 14.52; S, 11.08. Found: C, 62.37; H, 6.491; N, 14.48; S, 11.19.

4.1.3.5. 3-(2-Furyl)-2-(*N*-phenyllthiocarbamoyl)-3,3a,4,5,6,7-hexahydro-2*H*-indazol (1e). A white needles with a yield of 73% and recrystallized from ethanol. Mp 157–8 °C. **UV** (CH_3OH) nm: 203 (log ε: 4.44) and 278 nm. (log ε: 4.36); *IR* (KBr) cm^{-1}; 3490, 3189, 2937, 2856, 1636, 1509, 1329, 1214, 1147, 1089; ^1H NMR (DMSO-d_6, 400 MHz) δ (ppm) (*J* in Hz): 1.40–1.60 (3H; m; H_{4ax}, H_{5ax}, H_{6ax}), 1.75 (1H; m; H_{4eq}), 2.03 (1H; m; H_{5eq}), 2.15 (1H; m; H_{6eq}), 2.45 (1H; m; H_{7ax}), 2.60 (1H; d; H_{7eq}), 3.12 (1H; m; H_{3a}), 5.41 (1H; d; H_3; *J*: 5.2), 6.28 (1H; d; furan H_4), 6.39 (1H; dd; furan H_3), 7.10 (1H; m; furan H_5), 7,26 (2H; m; phenyl), 7.54 (3H; m; phenyl), 9.88 (1H; s; NH); **MS** (70 eV, EI): *m*/*e* (%): 325 (M^+, 100%), 257 (M−C_4H_4O, %28), 243 (M−C_6H_{10}, %37), 229 (M−$C_6H_{10}N$%60.34), 81 (M−$C_{13}H_{14}N_3S$, %34.21), 77 (M−$C_{12}H_{14}N_3OS$%51.72). Anal. Calcd for $C_{18}H_{19}N_3OS$: C, 66.43; H, 5.88; N, 12.91; S, 9.85. Found: C, 66.26; H, 5.504; N, 13.02; S, 9.54.

4.1.3.6. 3-(2-Thienyl)-2-thiocarbamoyl-2,3,4,5,6,7-hexahydro-1*H*-indazol (2a). A yellow solid substance with a yield of 55% and recrystallized from methanol. Mp 191–2 °C. *UV* (CH_3OH) nm: 202 (log ε: 4.31) and 344 nm. (log ε: 4.37); *IR* (KBr) cm^{-1}; 3401, 3236, 31, 2926,2861, 1585, 1500, 1278, 1205, 1071; ^1H NMR (DMSO-d_6, 400 MHz) δ (ppm): 1.63 (4H; m; H_{5ax}, H_{5eq}, H_{6ax}, H_{6eq}), 2.50 (6H; m; H_{4ax}, H_{4eq}), 2.63 (2H; m; H_{7ax}, H_{7eq}), 7.14 (H; dd; furan H_3), 7.30 (1H; d; furan H_4), 7.65 (2H; m; H_3-furan H_5), 7.90 and 8.27 (1H; sb; NH_2), 9.97 (1H; s; H_1); *MS* (70 eV, EI): *m*/*e* (%):265 (M^+, %64.03), 232 (M−SH, %39.60), 205 (M−$CSNH_2$, %98.52), 189(,100%), 169 (M−$C_6H_{10}N$, %25.74), 123 (M−$C_6H_{10}N_2S$, %33.61), 97 (M−$C_7H_{10}N_3S$, %30). Anal. Calcd for $C_{12}H_{15}N_3S_2$: C, 54.31; H, 5.70; N, 15.83; S, 24.16. Found: C, 54.35; H, 5.756; N, 15.71; S, 24.02.

4.1.3.7. 3-(2-Thienyl)-2-(*N*-methylthiocarbamoyl)-3,3a,4,5,6,7-hexahydro-2*H*-indazol (2b). A dirty white solid substance with a yield of 50% and recrystallized from methanol. Mp 177–8 °C. *UV* (CH_3OH) nm: 201 (log ε: 4.29), 245 (log ε: 4.20) and 274 nm. (log ε:4.29); *IR* (KBr) cm^{-1}; 3361, 3066, 2952, 2940, 2865, 16, 15, 1345, 1232, 1133, 1106; ^1H NMR (DMSO-d_6, 400 MHz) δ (ppm) (J in Hz): 0.60 (1H; dq; H_{4ax}), 1.11 (1H; m; H_{5ax}), 1.32 (1H; m; H_{6ax}) 1.65 (2H; m; H_{4eq}, H_{5eq}), 1.89 (1H; m; H_{6eq}), 2.28 (1H; dt; H_{7ax}), 2.60 (1H; d; H_{7eq}), 2.87 (3H; d; $-CH_3$), 3.40 (1H; m; H_{3a}), 6.09 (1H; d; H_3; *J*: 10.8), 6.76 (1H; d; thiophene H_4), 6.94 (1H; dd; thiophene H_3), 7.33 (1H; m; thiophene H_5),, 8.18 (1H; q; NH); *MS* (70 eV, EI): *m*/*e* (%): 279 (M^+, %68), 246 (M−SH, %49), 197 (M−C_6H_{10}, %28), 183 (M−$C_6H_{10}N$, 100%), 123 (M−$C_7H_{12}N_2S$, %18), 97 (M−$C_8H_{12}N_3S$, %19). Anal. Calcd for $C_{13}H_{17}N_3S_2$: C, 55.88; H, 6.13; N, 15.04; S, 22.95. Found: C, 55.05; H, 6.304; N, 14.99; S, 22.97.

4.1.3.8. 3-(2-Thienyl)-2-(*N*-ethylthiocarbamoyl)-3,3a,4,5,6,7-hexahydro-2*H*-indazol (2c). A white solid substance with a yield of 51% and recrystallized from methanol. Mp 194 °C. *UV* (CH_3OH) nm: 201 (log ε: 4.33), 246 (log ε: 4.24) and 275 nm. (log ε:4.24); *IR* (KBr) cm^{-1}; 3356, 3075, 2974, 2940, 2863, 1643, 1528, 1320, 1228, 1149, 1110; ^1H NMR (DMSO-d_6, 400 MHz) δ (ppm) (*J* in Hz): 0.60 (1H; dq; H_{4ax}), 1.06 (3H; t; $-CH_3$), 1.10–1.40 (2H; m; H_{5ax}, H_{6ax}), 1.60–1.70 (2H; m; H_{4eq}, H_{5eq}), 1.90 (1H; m; H_{6eq}), 2.28 (1H; dt; H_{7ax}), 2.60 (1H; dd; H_{7eq}), 3.40 (1H; m; H_{3a}), 3.50 (2H; m; $-CH_2-$), 6.10 (1H; d; H_3; *J*: 11.2), 6.76 (1H; d; thiophene H_4), 6.95 (1H; dd; thiophene H_3), 7.33 (1H; m; thiophene H_5), 8.18 (1H; t; NH); ^1H NMR ($CDCl_3$, 400 MHz) δ (ppm) (*J* in Hz): 0.85 (1H; dq; H_{4ax}), 1.24 (3H; t; $-CH_3$), 1.27–1.41 (2H; m; H_{5ax}, H_{6ax}), 1.72–1.79 (2H; m; H_{4eq}, H_{5eq}), 1.97 (1H; m; H_{6eq}), 2.20 (1H; dt; H_{7ax}), 2.72 (1H; dd; H_{7eq}), 3.24 (1H; m; H_{3a}), 3.64 (2H; m; $-CH_2-$), 6.20 (1H; d; H_3; *J*: 11.2), 6.80 (1H; d; thiophene H_4), 6.95 (1H; dd; thiophene H_3), 7.17 (1H; m; thiophene H_5), 7.27 (1H; t; NH); ^{13}C NMR (400 mHz, $CDCl_3$) δ (ppm); 15 (CH_3), 24 (C_5), 25 (C_6), 27.2 (C_4), 27.8 (C_7), 39 (CH_2), 50 (C_{3a}), 62 (C_3), 124.1 (thiophene-C_5), 124.7 (thiophene-C_4), 127 (thiophene-C_3), 1 (C_{7a}), 161 (thiophene-C_2), 175 (C=S); *HSQC* (^1H–^{13}C NMR)($CDCl_3$): 1.24/15 (CH_3/CH_3) 0.85, 1.72–1.79/27.2 (H_{4ax}, H_{4eq}–C_4), 1.27–1.41, 1.72–1.79 /24 (H_{5ax}, H_{5eq}/C_5), 1.27–1.41, 1.97/25 (H_{6ax}, H_{6eq}/C_6), 2.20, 2.72/27.8 (H_{7ax}, H_{7eq}/C_7), 3.24/50 (H_{3a}-C_{3a}), 3.64/39 ($-CH_2-$/$-CH_2-$), 6.20/62 (H_3/C_3), 6.95/127 (thiophene H_3/thiophene C_3), 6.80/124.7 (thiophene H_4/thiophene C_4), 7,17/124.1 (thiophene H_5/thiophene C_5); *MS* (70 eV, EI): *m*/*e* (%): 293 (M^+, 100%), 260 (M−SH, %59.13), 197 (M−$C_6H_{10}N$, %90.32), 123 (M−$C_8H_{14}N_2S$, %32.57), 97 (M−$C_9H_{14}N_3S$, %30.43), 44 (M−$C_{12}H_{13}N_2S_2$, %55.91). Anal. Calcd for $C_{14}H_{19}N_3S_2$: C, 57.30; H, 6.53; N, 14.32; S, 21.85. Found: C, 57.44; H, 6.307; N, 14.26; S, 21.82.

4.1.3.9. 3-(2-Thienyl)-2-(*N*-allylthiocarbamoyl)-3,3a,4,5,6,7-hexahydro-2*H*-indazol (2d). A white solid substance with a yield of 42% and recrystallized from methanol. Mp 181–2 °C. *UV* (CH_3OH) nm: 201 (log ε: 4.26), 246 (log ε: 4.15) and 275 nm. (log ε: 4.23); *IR* (KBr) cm^{-1}; 3360, 3074, 2975, 2938, 2860, 16, 1526, 1320, 1257, 1116, 1149; ^1H NMR (DMSO-d_6, 400 MHz) δ (ppm) (*J* in Hz): 0.60 (1H; dq; H_{4ax}), 1.11 (1H; tq; H_{5ax}), 1.32 (1H; m; H_{6ax}) 1.65 (2H; m; H_{4eq}, H_{5eq}), 1.89 (1H; m; H_{6eq}), 2.29 (1H; dt; H_{7ax}), 2.61 (1H; d; H_{7eq}), 3. (1H; m; H_{3a}), 4.09 (2H; m; $-CH_2-$), 5.06 (2H; dq; $=CH_2$), 5.84 (1H; m; $-CH=$), 6.10 (1H; d; H_3; *J*: 10.8), 6.77 (1H; d; thiophene H_4), 6.94 (1H; dd; thiophene H_3), 7.33 (1H; d; thiophene H_5), 8.27 (1H; t; NH); **MS** (70 eV, EI): *m*/*e* (%): 305 (M^+, %55.07), 290 (M−CH_3, %45.63), 272 (M−SH, %84.05), 249 (M−C_3H_6N, %88.40), 123 (M−$C_9H_{14}N_2S$, 100%), 97 (M−$C_{10}H_{14}N_3S$%66.66). Anal. Calcd for

$C_{15}H_{19}N_3S_2$: C, 58.98; H, 6.27; N, 13.76; S, 20.99. Found: C, 59.17; H, 6.086; N, 13.73; S, 21.05.

4.1.3.10. 3-(2-Thienyl)-2-(*N*-phenylthiocarbamoyl)-3,3a,4,5,6,7-hexahydro-2*H*-indazol (2e). A yellowish white solid substance with a yield of 70% and recrystallized from methanol. Mp: 140–1 °C. **UV** (CH_3OH) nm: 202 (log ε: 4.50) and 278 nm (log ε: 4.32); **IR** (KBr) cm^{-1}; 3313, 3059, 2941, 2855, 1640, 1516, 1330, 1229, 1192, 1152; ^{1}H NMR (DMSO-d_6, 400 MHz) δ (ppm) (*J* in Hz): 1.50 (3H; m; H_{4ax}, H_{5ax}, H_{6ax}), 1.75 (1H; m; H_{4eq}), 2.03 (1H; m; H_{5eq}), 2.22 (1H; m; H_{6eq}), 2.45 (1H; m; H_{7ax}), 2.60 (1H; m; H_{7eq}), 3.05 (1H; m; H_{3a}), 5.65 (1H; d; H_{3trans}; *J*: 4.8), 6.22 (1H; d; H_{3cis}; *J*: 11.2), 6.98 (1H; m; thiophene H_4), 7.10 (1H; m; thiophene H_3), 7,28 (2H; m; phenyl), 7.37 (1H; m; thiophene H_5), 7.54 (3H; m; phenyl), 9.96 (1H; s; NH); **MS** (70 eV, EI): *m*/*e* (%): 341 (M^+, %59.09), 308 (M−SH, 100%), 259 (M−C_6H_{10}, %21.81), 245 (M−$C_6H_{10}N$, %79.09), 205 (M−C_7H_6NS, %26.36). Anal. Calcd for $C_{15}H_{19}N_3S_2$: C, 63.31; H, 5.61; N, 12.30; S, 18.78. Found: C, 63.48; H, 5.457; N, 12.29; S, 18.86.

4.2. Single crystal X-ray crystallographic data of 1e

The data collection was performed on a STOE IPDS-II diffractometer with graphite-monochromated MoKα radiation (λ = 0.71073 Å) at 296 K. Crystallographic and refinement parameters are summarized in Table 1.

The structure was solved by direct methods using SHELXS-97[37] and refined by full-matrix least-squares procedures on F^2, using the program SHELXL-97.[37] All non-hydrogen atoms were refined anisotropically. All hydrogen atom positions were refined using a riding model. An empirical w scan absorption correction was applied. Molecular diagram (Fig. 2) was created using ORTEP-III.[38] Geometric calculations were performed with PLATON.[39]

Crystallographic data for compound **1e** reported in this paper have been deposited with the Cambridge Crystallographic Data Centre as supplementary publication number CCDC 717517. Copies of the data can be obtained, free of charge, on application to CCDC, 12 Union Road, Cambridge CB2 1EZ, UK (fax: +44 (0)1223-336033 or e-mail: deposit@ccdc.cam.ac.uk).

4.3. Biochemistry

All chemicals used were purchased from Sigma–Aldrich Co. (Germany).

4.3.1. Isolation of MAO from rat liver homogenates

The ethics Committee of Laboratory Animals at Hacettepe University, Turkey (2001/25-4), approved the animal experimentation. MAO was purified from the rat liver according to the Holt method with some modifications.[40] Liver tissue was homogenized 1:40 (w/v) in 0.3 M sucrose. Following centrifugation at 1000*g* for 10 min, the supernatant was centrifuged at 10,000*g* for 30 min to obtain crude mitochondrial pellet. The pellet was incubated with CHAPS of 1% at 37 °C for 60 min and centrifuged at 1000*g* for 15 min. Pellet was resuspended in 0.3 M sucrose and was layered onto 1.2 M sucrose, centrifuged at 53,000*g* for 2 h and resuspended in potassium phosphate buffer, pH 7.4, kept at −70 °C until used.

4.3.2. Measurement of MAO activity

Total MAO activity was measured spectrophotometrically according to the Holt method.[40] The assay mixture contained a chromogenic solution consisting of 1 mM vanillic acid, 500 μM 4-aminoantipyrine, and 4 U ml^{-1} peroxidase type II in 0.2 M potassium phosphate buffer, pH 7.6. The assay mixture contained 167 μl chromogenic solution, 667 μl substrate solution (500 μM *p*-tyramine) and 133 μl potassium phosphate buffer, pH 7.6. The mixture was preincubated at 37 °C for 10 min before the addition of enzyme. The reaction was initiated by adding the homogenate (100 μl), and an increase in absorbance was monitored at 498 nm at 37 °C for 60 min. A molar absorption coefficient of 4654 M^{-1} cm^{-1} was used to calculate the initial velocity of the reaction. Results were expressed as nmol h^{-1} mg^{-1}.

4.3.3. Selective measurement of MAO-A and MAO-B activities

Homogenates were incubated with the substrate *p*-tyramine (500 μM to measure MAO-A and 2.5 mM to measure MAO-B) following the inhibition of one of the MAO isoforms with selective inhibitors. Aqueous solution of clorgyline or pargyline (50 μM), as selective MAO-A and -B inhibitors were added to homogenates at the ratio of 1:100 (v/v), yielding the final inhibitor concentrations of 0.50 μM. Homogenates were incubated with these inhibitors at 37 °C for 60 min prior to activity measurement. After incubation of homogenates with selective inhibitors, total MAO activity was determined by the method described above.

4.3.4. Analysis of the kinetic data

Newly synthesized compounds were dissolved in dimethyl sulfoxide (DMSO), to a maximum concentration of 1% and used in the concentration range of 1–1000 μM. Inhibitors were incubated with the purified MAO at 37 °C for 0–60 min prior to adding them to the assay mixture. The reversibility of the inhibition of the enzyme by novel compounds was assessed by dialysis performed over 24 h at 37 °C relative to a potassium phosphate buffer, pH 7.6 capable of restoring 98–100% of the enzyme activity.

Kinetic data for interaction of the enzyme with the compounds were determined using the Microsoft Excel package program. The inhibitory activities of the novel compounds for MAO-A and -B were determined at 37 °C after incubation of the homogenates (previously treated with clorgyline for MAO-A or –B measurement) with the compounds for 60 min. Lineweaver–Burk plots were used to estimate the inhibition constant (K_i) of the inhibitors. IC_{50} values were determined from plots of residual activity percentage, calculated in relation to a sample of the enzyme treated under the same conditions without inhibitor, versus inhibitor concentration [*I*]. IC_{50} values were determined using non-linear regression analysis according to the equation for a sigmoid plot. Logarithmic transformation was also used for the determination of IC_{50} values for some compounds which showed their inhibition in a large concentration range.

4.3.5. Protein determination

The protein was determined according to the Bradford method,[41] in which bovine serum albumin was used as a standard.

4.4. Molecular docking

4.4.1. Protein setup

MAO-A (pdb code: 2z5x, resolution: 2.2 Å, cocrystalized with harmine) and MAO-B (pdb code: 1s3e, resolution: 1.6 Å, cocrystalized with the inhibitor 6-hydroxy-*N*-propargyl-1(*R*)-aminoindan) were obtained from the Protein Data Bank (http://www.rcsb.org).[12,14,15,42,43] Studies were carried out on only one subunit of the enzymes. The pdb files were edited and the β-chains were removed together with their irreversible inhibitors. All the water and all non-interacting ions were also removed.

4.4.2. Simulations of enzymes

Cleaned MAO-A and MAO-B and their cofactors FAD are equilibrated via energy minimization and Molecular Dynamics (MD) using NAMD v2.6 simulation package.[44] MD simulations were performed at constant NPT at 310 K using Langevin dynamics for all

non-hydrogen atoms, with a Langevin damping coefficient of 5 ps^{-1}. The system was kept at a constant pressure of 1 atm by using a Nose–Hoover Langevin piston[45] with a period of 100 fs and damping timescale of 50 ps. To simulate the cytoplasmic environment, the system was first solvated in a water box with dimensions of 107.6 Å × 96.5 Å × 84.2 Å and ions are added to make the overall system neutral using the plug-ins of VMD molecular visualization program (http://www.ks.uiuc.edu/Research/vmd).[46] The system is comprised of the protein and its cofactor with 8253 atoms, 74458 water molecules and 4 ions.

CHARMM22 forcefield[47,48] was used to describe the interaction potential of the protein, and waters are treated explicitly using TIP3P model.[49] Long-range electrostatic interactions were treated by the particle mesh Ewald (PME) method with a grid point density of over 1/Å. A cutoff of 12 Å was used for van der Waals and short-range electrostatics interactions; a switching function was started at 10 Å for van der Waals interactions to ensure a smooth cutoff. Simulation was performed under periodic boundary conditions to prevent surface effects. The hydrogen–oxygen and hydrogen–hydrogen distances in waters are constrained to the nominal length or angle specified in the parameter file, making the water molecules completely rigid. Also, the bond between each hydrogen and the (one) atom to which it is bonded is similarly constrained.

Time step was 2 fs and the data was taken every 1 ps. The number of time steps between each full electrostatics evaluation is set to 2. Short-range non-bonded interactions are calculated every time step.

Prior to Molecular Dynamics, the system was subjected to 10,000 steps of energy minimization using conjugate gradient algorithm. A total of 10 ns of Molecular Dynamics simulation was then carried out on a IntelliStation Z Pro workstation with 2 dual core Intel Xeon 5160 processors (total of 6 GHz and 4 GiB memory). The last snapshot at the tenth nanosecond was then used for docking studies.

The AUTODOCKTOOLS (ADT),[50] graphical user interface, program was employed to setup the enzymes: all hydrogens were added, Gasteiger[51] charges were calculated and non-polar hydrogens were merged to carbon atoms. For macromolecules, generated pdbqt files were saved.

4.4.3. Ligand setups

The 3D structures of ligand molecules were built, (optimized to the (PM3) level), and saved in pdb format with the aid of the molecular modeling program Spartan (Wavefunction Inc.).[52] The AUTODOCKTOOLS package was also employed here to generate the docking input files of ligands. AUTODOCK 4.01 was employed for all docking calculations.[53,54] The AUTODOCKTOOLS (ADT)-generated input files were used in dockings. In all docking a grid box size of 80 × 80 × 80 points in *x*, *y*, and *z* directions was built, and because the location of the inhibitor in the complex was known, the maps were centered on the N5 atom of FAD in the catalytic site of the protein. A grid spacing of 0.375 Å (approximately one forth of the length of a carbon–carbon covalent bond) and a distances-dependent function of the dielectric constant were used for the calculation of the energetic map. Ten runs were generated by using Lamarckian genetic algorithm searches. Default settings were used with an initial population of 50 randomly placed individuals, a maximum number of 2.5×10^7 energy evaluations, and a maximum number of 2.7×10^4 generations. A mutation rate of 0.02 and a crossover rate of 0.8 were chosen. Results differing by less than 0.5 Å in positional root-mean-square deviation (RMSD) were clustered together and the results of the most favorable free energy of binding were selected as the resultant complex structures. From the 'Estimated Free Energy of Binding' (kcal/mol) program calculates the inhibition constants taking into consideration of the dissociation of the enzyme inhibitor complex using basic thermodynamics formula of $\Delta G = RT \ln K_i$.

The resultant structure files were analyzed by using DISCOVERY STUDIO VISUALIZER 2.1 (http://accelrys.com) visualization program.

Acknowledgment

This study was supported by the Hacettepe University Research Fund (08D09301002 (4686)).

References and notes

1. Mondovi, B. Structure and Function of Amine Oxidases, CRC Press, Boca Raton, FL, 1985.
2. Westlund, K. N.; Denney, R. M.; Kochersperger, L. M.; Rose, R. M. *Science* **1985**, *230*, 181.
3. Westlund, K. N.; Denney, R. M.; Rose, R. M.; Abell, C. W. *Neuroscience* **1988**, *25*, 439.
4. Bousquet, P.; Feldman, J.; Schwartz, J. *J. Pharmacol. Exp. Ther.* **1984**, *230*, 232.
5. Grimsby, J.; Lan, N. C.; Neve, R.; Chen, K.; Shih, J. C. *J. Neurochem.* **1990**, *55*, 1166.
6. Rudorfer, M. V.; Potter, W. Z. *Drugs* **1989**, *37*, 713.
7. Pacher, P.; Kohegyi, E.; Keckemetti, V.; Furst, S. *Curr. Med. Chem.* **2001**, *8*, 89.
8. Pacher, P.; Keckemetti, V.; Furst, S. *Curr. Med. Chem.* **2004**, *11*, 925.
9. Wouters, J. *Curr. Med. Chem.* **1998**, *5*, 137.
10. Tetrud, J. W.; Langston, J. W. *Neurology* **1989**, *39*, 1483.
11. Carreiras, M. C.; Marco, J. L. *Curr. Pharm. Des.* **2004**, *10*, 3167.
12. Binda, C.; Newton-Vinson, P.; Hubálek, F.; Edmondson, D. E.; Mattevi, A. *Nat. Struct. Biol.* **2002**, *9*, 22.
13. Edmondson, D. E.; Binda, C.; Mattevi, A. *Neurotoxicology* **2004**, *25*, 63.
14. De Colibus, L.; Li, M.; Binda, C.; Lustig, A.; Edmondson, D. E.; Mattevi, A. P. *Natl. Acad. Sci. U.S.A.* **2005**, *102*, 12684.
15. Binda, C.; Hubálek, F.; Li, M.; Edmondson, D. E.; Mattevi, A. *FEBS Lett.* **2004**, *564*, 225.
16. Binda, C.; Edmondson, D. E.; Mattevi, A. *J. Biol.Chem.* **2002**, *277*, 23973.
17. Hubálek, F.; Binda, C.; Khalil, A.; Li, M.; Mattevi, A.; Castagnoli, N.; Edmondson, D. E. *J. Biol. Chem.* **2005**, *280*, 15761.
18. Tipton, K. F. *Biochem. J.* **1972**, *128*, 913.
19. Mc Kenna, K. F.; Baker, G. B.; Coutta, R. T. N. S. *Arch. Pharmacol.* **1991**, *343*, 478.
20. Yamada, N.; Takahashi, S.; Todd, K. G.; Baker, G. B.; Paetsch, P. R. *J. Pharm. Sci.* **1993**, *82*, 934.
21. Belleau, B.; Moran, J. *J. Med. Pharm. Chem.* **1962**, *5*, 215.
22. Parmar, S. S.; Pandey, B. R.; Dwivedi, C.; Harbison, R. D. *J. Pharm. Sci.* **1974**, *63*, 1152.
23. Manna, F.; Chimenti, F.; Bolasco, A.; Bizzarri, B.; Befani, O.; Pietrangeli, P.; Mondovi, B.; Turini, P. *J. Enzyme Inhib.* **1998**, *13*, 207.
24. Manna, F.; Chimenti, F.; Bolasco, A.; Secci, D.; Bizzarri, B.; Befani, O.; Turini, P.; Mondovi, B.; Alcaro, S.; Tafi, A. *Bioorg. Med. Chem. Lett.* **2002**, *12*, 3629.
25. Gökhan, N.; Yeşilada, A.; Uçar, G.; Erol, K.; Bilgin, A. A. *Arch. Pharm.* **2003**, *336*, 362.
26. Chimenti, F.; Maccioni, E.; Secci, D.; Bolasco, A.; Chimenti, P.; Granese, A.; Befani, O.; Turini, P.; Alcaro, S.; Ortuso, F.; Cirilli, R.; La Torre, F.; Cardia, M. C.; Distinto, S. *J. Med. Chem.* **2005**, *48*, 7113.
27. Gökhan Kelekçi, N.; Yabanoğlu, S.; Küpeli, E.; Salgın Gökşen, U.; Özgen, Ö; Uçar, G.; Yeşilada, E.; Kendi, E.; Yeşilada, A.; Bilgin, A. A. *Bioorg. Med. Chem.* **2007**, *15*, 5775.
28. Yeşilada, A.; Gökhan, N.; Özer, İ.; Vural, K.; Erol, K. *Farmaco* **1996**, *51*, 775.
29. Uçar, G.; Gökhan, N.; Yeşilada, A.; Yabanoğlu, S.; Bilgin, A. A. *Hacettepe Univ., J. Faculty Pharm.* **2005**, *25*, 23.
30. Yabanoğlu, S.; Uçar, G.; Gökhan, N.; Salgın, U.; Yeşilada, A.; Bilgin, A. A. *J. Neural. Transm.* **2007**, *114*, 769.
31. Gökhan-Kelekçi, N.; Koyunoğlu, S.; Yabanoğlu, S.; Yelekçi, K.; Özgen, Ö.; Uçar, G.; Erol, K.; Kendi, E.; Yeşilada, A. *Bioorg. Med. Chem.* **2009**, *17*, 675.
32. Hassner, A.; Michelson, M. J. *J. Org. Chem.* **1962**, *27*, 298.
33. Cremer, D.; Pople, J. A. *J. Am. Chem. Soc.* **1975**, *97*, 1354.
34. Youdim, M. B. H.; Edmondson, D.; Tipton, K. F. *Nat. Rev. Neurosci.* **2006**, *7*, 295.
35. Fierro, A.; Osorio-Olivares, M.; Cassels, B. K.; Edmondson, D. E.; Sepulveda-Boza, S.; Reyes-Parada, M. *Biiorg. Med. Chem.* **2007**, *15*, 5198.
36. Walton, H. M. *J. Org. Chem.* **1957**, *22*, 1161.
37. Sheldrick, G. M. SHELXS97 and SHELXL97, Program for Crystal Structure Solution, University of Göttingen: Germany, 1997.
38. Farrugia, L. *J. Appl. Crystallogr.* **1997**, *30*, 565.
39. Spek, A. L. *PLATON—A Multipurpose Crystallographic Tool*; Utrecht: Utrecht University, The Netherlands, 2005.
40. Holt, A.; Sharman, D. F.; Baker, G. B.; Pelcic, M. M. *Anal. Biochem.* **1997**, *244*, 384.
41. Bradford, M. M. *Anal. Biochem.* **1976**, *72*, 248.
42. Binda, C.; Hubalek, F.; Li, M.; Herzig, Y.; Sterling, J.; Edmondson, D. E.; Mattevi, A. *J. Med. Chem.* **2004**, *47*, 1767.
43. Son, S. Y.; Ma, J.; Kondou, Y.; Yoshimura, M.; Yamashita, E.; Tsukihara, T. *Proc. Natl. Acad. Sci.* **2008**, *105*, 5739.
44. Phillips, J. C.; Braun, R.; Wang, W.; Gumbart, J.; Tajkhorshid, E.; Villa, E.; Chipot, C.; Skeel, R. D.; Kale, L.; Schulten, K. *J. Comput. Chem.* **2005**, *26*, 1781.
45. Feller, S. E.; Zhang, Y. H.; Pastor, R. W.; Brooks, B. R. *J. Chem. Phys.* **1995**, *103*, 4613.
46. Humphrey, W.; Dalke, A.; DalkeSchulten, K. *J. Mol. Graph.* **1996**, *14*, 33.
47. MacKerell, A. D., Jr.; Bashford, D.; Bellott, M.; Dunbrack, R. L., Jr.; Evanseck, J.; Field, M. J.; Fischer, S.; Gao, J.; Guo, H.; Ha, S., et al *FASEB J.* **1992**, *6*, A143.

48. MacKerell, A. D., Jr.; Bashford, D.; Bellott, M.; Dunbrack, R. L., Jr.; Evanseck, J.; Field, M. J.; Fischer, S.; Gao, J.; Guo, H.; Ha, S., et al *J. Phys. Chem.* **1998**, *102*, 3586.
49. Jorgensen, W. L.; Chandrasekhar, J.; Madura, J. D.; Impey, R. W.; Klein, M. L. *J. Chem. Phys.* **1983**, *79*, 926.
50. Michel, F.; Saner, P. *J. Mol. Graph. Model.* **1999**, *17*, 57.
51. Gasteiger, J.; Marsili, M. *Tetrahedron* **1980**, *36*, 3219.
52. Wavefunction, Inc. 18401 von Karman Avenue, Suite 370, Spartan'02, Irvine, CA 92612, USA.
53. Morris, G. M.; Goodsell, D. S.; Halliday, R. S.; Huey, R.; Hart, W. E.; Belew, R. K.; Olson, A. *J. Comput. Chem.* **1998**, *19*, 1639.
54. Huey, R.; Morris, G. M.; Olson, A. J.; Goodsell, D. S. *J. Comput. Chem.* **2007**, *28*, 1145.